NANO LETTERS

Letter

Cite This: *Nano Lett.* 2018, 18, 7777−7783

pubs.acs.org/NanoLett

Relaxation Dynamics of Zero-Field Skyrmions over a Wide Temperature Range

Licong Peng,[†,‡,§] Ying Zhang,[*,†,§] Liqin Ke,[§] Tae-Hoon Kim,[§] Qiang Zheng,[∥] Jiaqiang Yan,[∥] X.-G. Zhang,[⊥] Yang Gao,[#] Shouguo Wang,[#] Jianwang Cai,[†,‡] Baogen Shen,[†,‡] Robert J. McQueeney,[§] Adam Kaminski,[§] Matthew J. Kramer,[§] and Lin Zhou[*,§]

[†]Beijing National Laboratory for Condensed Matter Physics, Institute of Physics, Chinese Academy of Sciences, Beijing 100190, China

[‡]School of Physical Sciences, University of Chinese Academy of Sciences, Beijing 100049, China

[§]U.S. Department of Energy, Ames Laboratory, Ames, Iowa 50011, United States

[∥]Materials Science and Technology Division, Oak Ridge National Laboratory, Oak Ridge, Tennessee 37831, United States

[⊥]Department of Physics and the Quantum Theory Project, University of Florida, Gainesville, Florida 32611, United States

[#]Institute of Advanced Materials, Beijing Normal University, Beijing 100875, China

Supporting Information

ABSTRACT: The promise of magnetic skyrmions in future spintronic devices hinges on their topologically enhanced stability and the ability to be manipulated by external fields. The technological advantages of nonvolatile zero-field skyrmion lattice (SkL) are significant if their stability and reliability can be demonstrated over a broad temperature range. Here, we study the relaxation dynamics including the evolution and lifetime of zero-field skyrmions generated from field cooling (FC) in an FeGe single-crystal plate via in situ Lorentz transmission electron microscopy (L-TEM). Three types of dynamic switching between zero-field skyrmions and stripes are identified and distinguished. Moreover, the generation and annihilation of these metastable skyrmions can be tailored during and after FC by varying the magnetic fields and the temperature. This dynamic relaxation behavior under the external fields provides a new understanding of zero-field skyrmions for their stability and reliability in spintronic applications and also raises new questions for theoretical models of skyrmion systems.

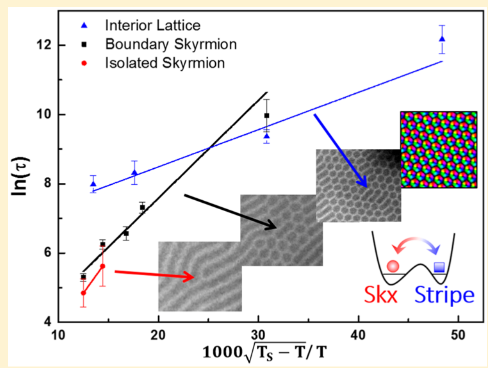

KEYWORDS: *Relaxation dynamics, zero-field skyrmions, activation energy, field cooling (FC), L-TEM, FeGe*

Magnetic skyrmions are topologically stable spin textures[1−3] originally introduced by Skyrme as a model to describe a state of nucleons.[4] Bogdanov and Yablonskii[5] theoretically predicted that magnetic vortices could exist in magnetically ordered crystals with a broken spatial inversion symmetry. It was then experimentally confirmed by Mühlbauer et al.[6] with neutron scattering in bulk MnSi. Subsequently, systematic real-space observations of skyrmion lattice (SkL) with high-resolution Lorentz transmission electron microscopy (L-TEM) in B20 magnets of metallic MnSi,[7] $Fe_{1-x}Co_xSi$,[8] FeGe,[9] and insulating Cu_2OSeO_3[10] led to significant breakthroughs in this field. In chiral magnets, the competition between the Dzyaloshinskii−Moriya interaction (DMI) due to the symmetry-broken crystal structure and the ferromagnetic exchange interaction favors noncollinear arrangements of spins, resulting in a long-period helical ground state with a fixed propagation wave-vector Q and a modulation period λ_m.[6,11−13] When applying external magnetic fields, the spiral phase is driven into a chiral skyrmion lattice with a triple-Q state, presenting a superposition of three helices at an angle of 120°.[6] Their peculiar topological configurations, intriguing emergent electromagnetic properties and low current-driven behavior,[2,14−17] make skyrmions a very promising platform for information storage and spintronic devices.[14,18,19]

However, equilibrium skyrmions typically exist within a narrow temperature range just below T_C and under a finite magnetic fields (B) in B20 compounds[7,8,14] (e.g., 260−273 K and 50−200 mT for an FeGe plate). Among these materials, FeGe has the highest Curie temperature ($T_C \sim 278$ K). In order to develop a platform for energy efficient data storage and processing, significant efforts have been devoted to extend the temperature range and to generate zero-field nonvolatile skyrmions.[16,20,21] For example, generic supercooling or field-

Received: September 2, 2018
Revised: November 10, 2018
Published: November 30, 2018

DOI: 10.1021/acs.nanolett.8b03553
Nano Lett. 2018, 18, 7777−7783

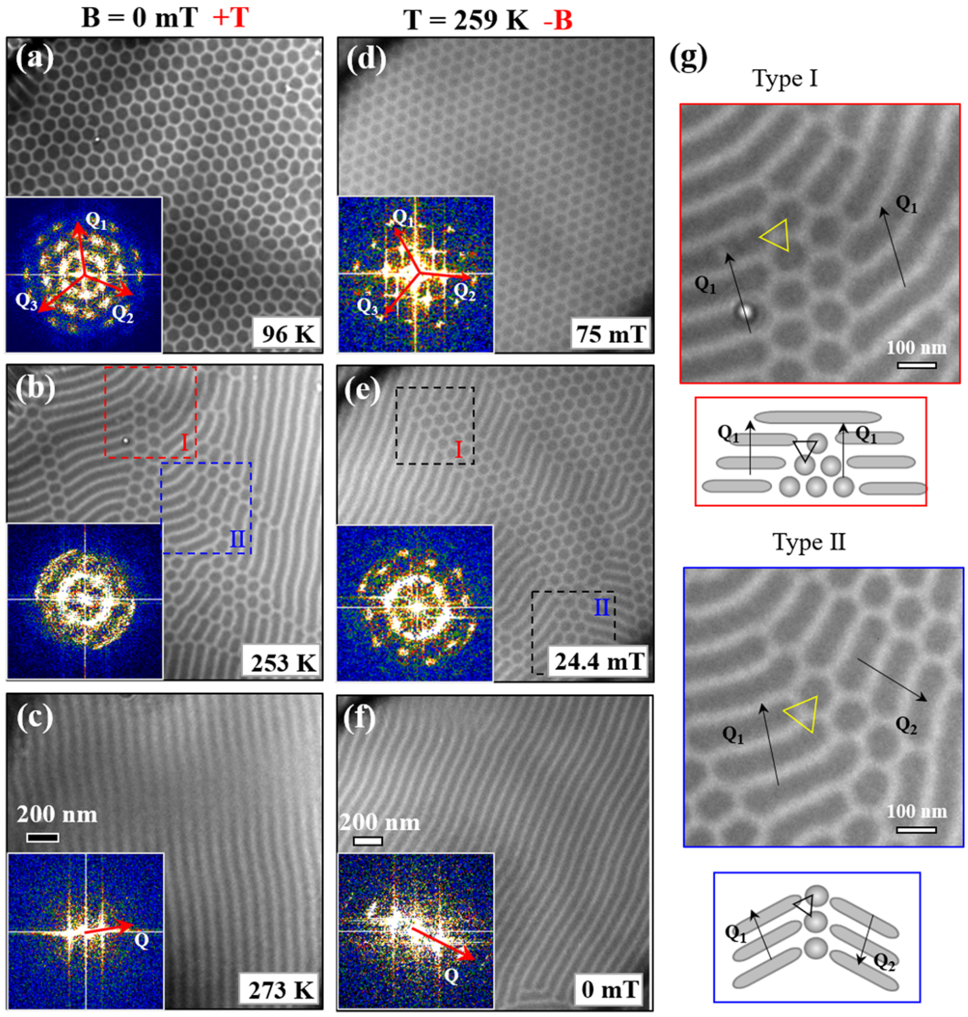

Figure 1. Magnetic evolution from SkL to helical stripes. (a) Zero-field SkL after 87.8 mT FC to 96 K and the evolution of the skyrmion lattice while increasing temperature to (b) 253 K and (c) 273 K. (d, e) Equilibrium SkL evolution at 259 K while decreasing the field to (d) 75 mT, (e) 24.4 mT, and (f) 0 mT. Insets in all panels: Fast Fourier Transform (FFT) of the images demonstrating the corresponding symmetric transformation. (g) Enlarged images obtained from (b) representing two growth modes illustrated by the corresponding schematics below each image.

cooling (FC) has been proved to be able to generate metastable skyrmions as studied via magnetization, ac susceptibility, Hall-resistivity measurements, and small-angle neutron scattering (SANS) in $Fe_{1-x}Co_xSi$,[22] MnSi,[23] and $Co_8Zn_8Mn_4$.[15] In contrast, real-space L-TEM imaging provides more elegant, direct, and high-resolution observations for skyrmion dynamics.[24−26] Zero-field skyrmions have been detected after FC manipulation via topological Hall-resistivity measurements in epitaxial FeGe (111) thin films[27] and were then visualized in (110) an FeGe thin plate by L-TEM.[28]

The magnetic field and temperature are the most critical controllable external fields for skyrmion stability. Therefore, the dynamics of metastable zero-field skyrmions, including their evolution behavior as a function of external fields, in particular the relaxation lifetime, is the key issue for any potential skyrmion-based applications. Recently, the dynamics of metastable zero-field skyrmions as a function of the external magnetic fields was found to have unique collapsing and aggregation behavior mainly between skyrmions and the conical phase.[28] Previous studies[15,23−26,29] interpreted experimental measurements and Monte Carlo simulations of a single skyrmion using the Arrhenius law with a fixed activation energy independent of the temperature. Such an assumption is due to scarcity of the data over limited temperature ranges for the existence and observation of the skyrmions.

In this work, we study the relaxation dynamics between metastable skyrmions and stripes under zero field over the wide temperature range between 96 and 263 K. By generating zero-field skyrmions over such a wide temperature range, we are able to conduct a systematic analysis on skyrmion switching dynamics using L-TEM. We find three distinct switching processes between the skyrmions and stripes depending on whether the skyrmions are isolated, interior SkL, or at the boundary of a SkL. The observed relaxation time for each switching process as a function of the temperature yields activation energies that are temperature-dependent, indicating a non-Arrhenius behavior. Thermal activation across energy barriers govern the lifetime of the topologically protected units, and by summarizing their dynamic behaviors, the lifetime of zero-field skyrmions as memory elements in computers and hard disks under different environments can be proposed.

Materials and Methods. Single crystals of bulk FeGe were grown by the chemical vapor transport technique.[30] A FeGe

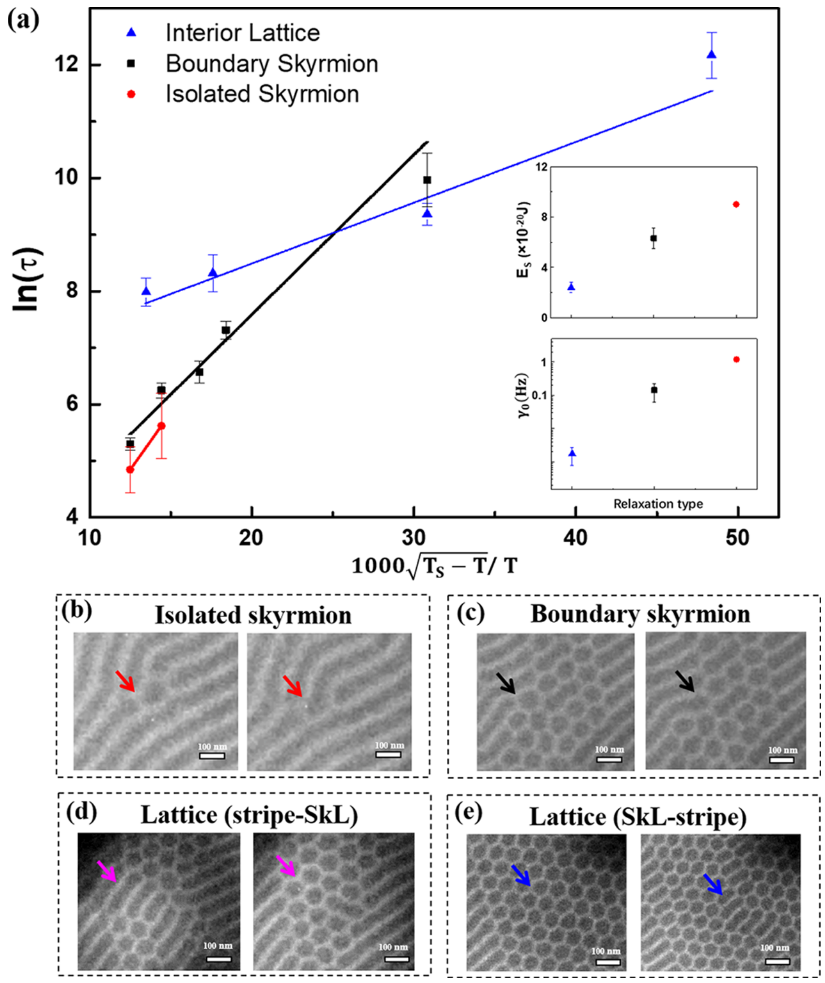

Figure 2. Relaxation dynamics of metastable zero-field skyrmions at different temperatures. (a) Linear fitting plots of $\ln(\tau)$ versus $\frac{1000\sqrt{T_S - T}}{T}$ for three switching processes based on direct real-space L-TEM observations. The switching processes are classified into (b) isolated skyrmion at 253 K, (c) boundary skyrmion at 250 K, (d) interior SKL stripe to SkL at 243 K, and (e) skyrmion to stripe at 218 K. The summary of the corresponding energy barriers E_s at 0 K and attempt frequencies in the insets of part a.

TEM thin plate with its surface normal to the [001] crystallographic direction was prepared by using a FEI Helios dual-beam focused-ion-beam (FIB) instrument. The crystal orientation was identified by the morphology of the single-crystal facets under an optical microscope and further confirmed by selected area electron diffraction (SAED). High-resolution high-angle-annular dark-field (HAADF) scanning transmission electron microscopy (STEM) and SAED were performed using a probe aberration-corrected FEI Titan Themis. All of the defocused L-TEM images of magnetic domains were recorded by using the Lorentz mode of a Tecnai F20 TEM. The TEM sample's temperature is controlled by using a liquid nitrogen cooling holder (Gatan model 636). The external magnetic field is applied along the electron beam direction by partially exciting the objective lens of the TEM, which is precalibrated with a Hall probe. The quantitative in-plane magnetizations of L-TEM Fresnel images are analyzed by a phase-retrieval QPt software on the basis of the transport of intensity equation (TIE).[31]

Results and Discussions. Zero-field SkL at low temperatures down to 96 K is generated by cooling a FeGe single-crystal plate under an 87.8 mT field using a liquid nitrogen holder in L-TEM mode. Based on these obtained zero-field SkLs at 96 K, the temperature is gradually increased, and the evolution from hexagonal SkL to stripes following two growth modes is observed as shown in Figure 1a−c. (See Figure S1 for more images in the Supporting Information.) The evolution starts with the formation of short dumbbell-shaped stripes (with a half-skyrmion pair at both ends of the stripe) and then followed by longer periodic lines with different Q-vectors at ~253 K (Figure 1b). When the temperature approaches T_C, the helical stripes with a single-Q (Figure 1c) finally substitute the triangular SkL with triple-Q modulation vectors (Figure 1a). The process for SkL diminishing is further verified by corresponding fast Fourier transform (FFT) diffraction patterns in the insets. The magnified regions (Figure 1g) from the selected red and blue squares in Figure 1b demonstrate two types of growth modes from skyrmions to stripes. In type I mode, the stripes around skyrmions have one single-Q, whereas, in type II mode, those stripes have double-Q, which are approximately 120° to each other. A previous study based on the mean-field approximation indicates that these types of growth modes are formed in order to minimize system energy.[6] These two growth modes are also observed for the equilibrium skyrmions as shown in Figure 1d−f but

DOI: 10.1021/acs.nanolett.8b03553
Nano Lett. 2018, 18, 7777−7783

not in the metastable zero-field skyrmions when decreasing the magnetic field.[28]

The zero-field skyrmion evolution over temperatures, specifically the skyrmion-stripe switching behavior, is monitored via video recording. The switching frequency varies by orders of magnitude over the temperature range. At 96 K, no switching is detected for hours. In contrast, a typical switching takes only a few seconds at 250 K (Figure S2). More interestingly, even at the same temperature, the switching rates differ greatly depending on the environment of the skyrmion that is being switched. We classify the switching process into three types according to the environment of the skyrmion, i.e., isolated skyrmions, boundary skyrmions, and interior skyrmions of a SkL. For each type, the average switching time is estimated using $\tau = \frac{Mt}{N}$, where N is the number of switching events over the observation time interval t and M is the total number of skyrmion sites for the same type under observation. These three types of switching processes are summarized in Figure 2. Other types of stripe-skyrmion switching do not occur in sufficient numbers to yield reliable statistics.

The relaxation time is usually fitted as a function of temperature using the Arrhenius law, $\tau = \tau_0 \exp\left(\frac{E_s}{k_B T}\right)$ where τ_0 is the pre-exponential factor (where $1/\tau_0$ defines the attempt frequency γ_0), k_B is the Boltzmann constant, and E_s is the activation energy, which is commonly assumed to be temperature-independent. However, assuming a temperature-independent activation energy for isolated skyrmions yields an unphysical attempt frequency of 3.4×10^{17} Hz. Furthermore, all data exhibit a downward curvature when plotting $\ln\tau$ as a function of $1/T$, suggesting a sublinear temperature dependence of the activation energy that diminishes near the skyrmion transition temperature. In order not to increase the number of fitting parameters, we assume a simple temperature-dependent activation energy $E_s = C\sqrt{T_S - T}$, where $T_S = 263$ K is the temperature at which metastable skyrmions completely disappear under zero field, as shown in the phase diagram of Figure 3h. This expression yields reasonable fits for all processes with physically meaningful attempt frequencies.

The skyrmion lattice switching processes (skyrmion to stripe and stripe to skyrmion) have similar rates and thus are fitted together as a single type. Insets of Figure 2a show the summarized zero temperature activation energies $C\sqrt{T_S}$ and the fitted attempt frequency γ_0. Here, the visually more stable interior skyrmions are associated with a lower attempt frequency despite a somewhat lower activation energy, similar to the simulation and experimental results on skyrmion stability in Pd/Fe/Ir(111).[29] The difference in activation energy causes the dominated switching to be interior skyrmions in a SkL at lower temperatures and to be isolated skyrmions at higher temperatures. The zero temperature activation energy is $(2.4 \pm 0.4) \times 10^{-20}$ J for interior skyrmion lattices and $(6.3 \pm 0.9) \times 10^{-20}$ J for the boundary skyrmions. These values are in the same magnitude with the previously reported skyrmion switching energy barrier of the metastable skyrmions via tuning the magnetic fields in $Fe_{1-x}Co_xSi$[24] and that in BaFeScMgO[26] but 3 orders of magnitude lower than 10^{-17} J of the skyrmions in LaBaMnO.[25]

The observed phenomena raise new questions for theoretical models, demanding that the complicated skyrmion environment in real material be considered instead of an ideal single

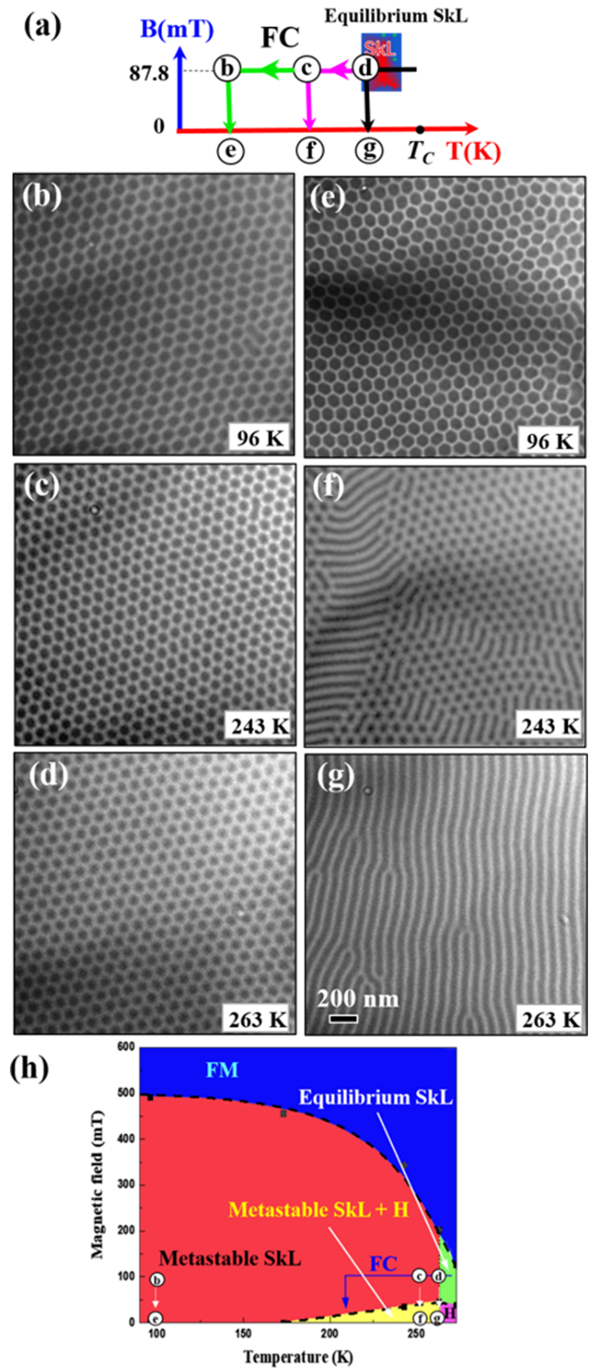

Figure 3. Realization of zero-field metastable SkL in FeGe directly observed by L-TEM. (a) Schematic illustration of the FC at 87.8 mT from the equilibrium SkL. FC to different temperatures: (b) 96 K, (c) 243 K, (d) 263 K. (e−g) Corresponding L-TEM images at zero field after FC. (h) Skyrmion distributions at different temperatures based on the FC procedure via in situ L-TEM. The metastable SkL state within a broad (T, B) range (red area) realized after FC from the equilibrium range (green area). Ferromagnetic state (blue area), helical region (pink area), and mixed states of metastable SkL and stripes (yellow area).

skyrmion picture[23−26] and the significant differences between stable and metastable skyrmions be taken into account. The question of a temperature-dependent activation energy that diminishes near T_S also needs theoretical understanding.

DOI: 10.1021/acs.nanolett.8b03553
Nano Lett. 2018, 18, 7777−7783

The optimized conditions to generate the zero-field skyrmion lattices are systematically studied in FeGe. FC under the magnetic field of 87.8 mT from 263 to 96 K (Figure 3) sustains the SkL even after the magnetic field is removed (Figure 3e). FC extends the SkL phase to a broad temperature region below T_C. A broader (T, B) region including the zero-field SkL phase (red area) and equilibrium skyrmion phase as a function of magnetic field is schematically illustrated as shown in Figure 3h based on L-TEM images. The removal of the magnetic field has different consequences if FC to different target temperatures. For example, skyrmions start to transform into stripes when removing the magnetic field at a temperature higher than 173 K (Figure S4). FC to higher target temperatures leads to either a mixed state (243 K, Figure 3f) or a complete helical phase (263 K, Figure 3g) at zero field.

The generation of the zero-field skyrmions depends strongly on the magnitude of the external magnetic field applied during the FC process, as shown in Figure 4. The highest density of zero-field SkL at 96 K is generated after FC at an optimum magnetic field of 87.8 mT (Figure 4c). In comparison, the complete stripe phase is formed if cooling without a magnetic field (Figure 4a), and a mixed stripe and skyrmion phase appears when FC at 49.8 mT (Figure 4b). Cooling at a higher magnetic field of 164 mT results in a mixed state of skyrmions and ferromagnetic state after the field is removed, as shown in Figure 4d. The different response behavior to external fields between the equilibrium skyrmions and zero-field metastable skyrmions is further observed. Similar to the equilibrium skyrmions, the diameter of metastable skyrmions also shrinks until their complete disappearance when increasing the external magnetic field. However, skyrmions cannot reappear once the metastable skyrmions have been completely transformed into stripes or a saturated ferromagnetic phase, which is in contrast with the reversible transition of equilibrium skyrmions. (See the comparison in Figure S5.) Unlike the equilibrium stripes, the metastable stripes obtained via FC cannot evolve into skyrmions under the magnetic fields as shown in Figure S6.

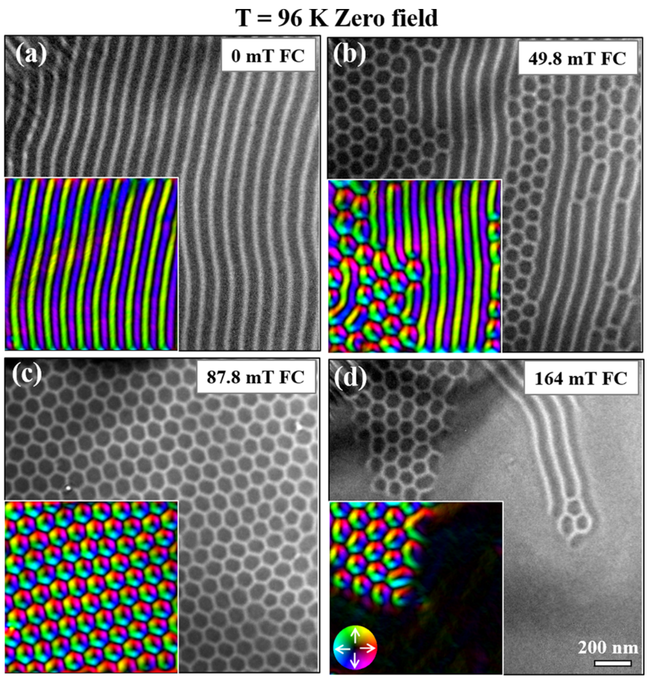

Figure 4. Effects of magnetic fields during FC on zero-field skyrmion density. (a) Only stripe domains after zero-field cooling (ZFC). (b) Mixed states of stripes and skyrmions after FC at 49.8 mT. (c) Well-distributed SkL with the highest density after FC at an optimum magnetic field of 87.8 mT, corresponding well with the critical magnetic field needed for equilibrium SkL generation. (d) Mixed states of stripes, skyrmions, and ferromagnetic state after FC at a high field of 164 mT.

HAADF-STEM imaging reveals a high-quality FeGe single crystal without discernible structural defects. The Fe−Ge dumbbells are clearly resolved when viewed along the [001] zone axis as shown in Figure 5a−c, consistent with the symmetry-broken B20 structure. This asymmetric structure determines the specific chirality of the skyrmion configuration as discussed in previous studies.[14] The slight thickness variation of the FeGe TEM sample in this study is shown in Figure S7, which contributes to the inhomogeneous distribution of the skyrmion lattices. The in-plane magnetization is investigated at 263 K, as shown in Figure 5d for the spontaneous stripe domains with a modulation length of λ_m ~ 75 nm and Figure 5e for the equilibrium SkL in a triangular pattern at an applied field of 87.8 mT, respectively. The observed crystal and magnetic configurations (Figure S8) for the equilibrium skyrmion phase in this single-crystal FeGe are consistent with previous results.[14]

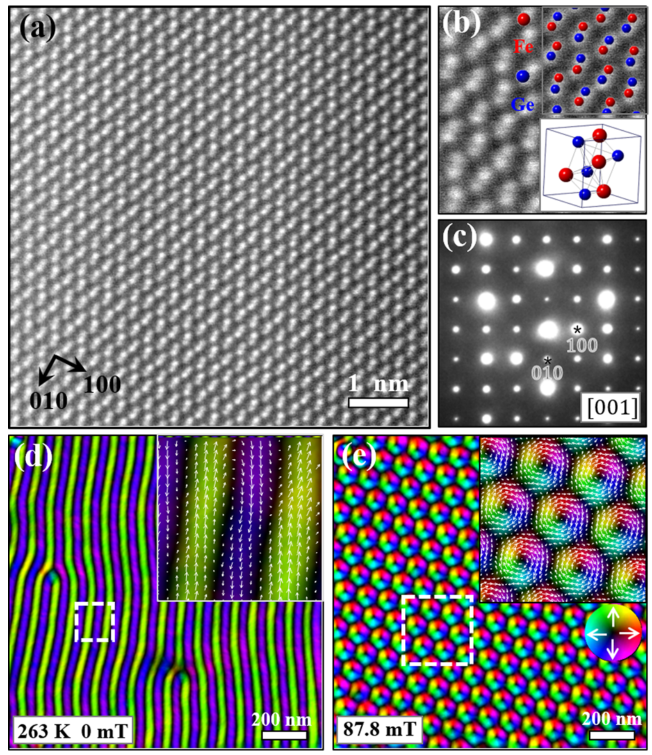

Figure 5. Crystal structure at room temperature and the equilibrium magnetic domains at 263 K in an FeGe single crystal. (a) High-resolution HAADF-STEM image of FeGe taken along the [001] zone axis. (b) Enlarged image from panel (a) revealing the Fe−Ge dumbbell in the cubic B20 structure. (c) Selected area electron diffraction pattern along the [001] zone axis. (d, e) Magnetic domain configuration via the TIE method of (d) helical ground state and (e) skyrmion lattice at a magnetic field of 87.8 mT.

In summary, a comprehensive and quantitative study on skyrmion-stripe switching behavior and dynamics of zero-field

DOI: 10.1021/acs.nanolett.8b03553
Nano Lett. 2018, 18, 7777−7783

skyrmions after different FC processes is carried out over a broad temperature range using in situ L-TEM. Three distinct temperature-dependent switching processes are identified. The switching behaviors are characterized by temperature-dependent activation energies, suggesting a non-Arrhenius law behavior. The growth modes from zero-field SkLs to stripes when increasing temperature is similar to the equilibrium skyrmion evolution while decreasing the magnetic field, however, the metastable skyrmions have a unique phase transition between the stripe and saturated ferromagnetic phase unlike the reversible transition of equilibrium skyrmions. Comprehensive understanding the dynamics and lifetime of zero-field skyrmions provides a database for the stability and reliability of future skyrmion-based spintronics under external fields and raises new questions to theoretical models.

ASSOCIATED CONTENT

Supporting Information

The Supporting Information is available free of charge on the ACS Publications website at DOI: 10.1021/acs.nanolett.8b03553.

> Magnetic configuration analysis; extended SkL phase after FC; metastable SkL dependence on the temperature and different FC processes; reversible equilibrium phase and irreversible nonequilibrium phase; relaxation dynamics by in situ L-TEM and the calculation of the energy barrier and attempt frequency; sample thickness by EELS (PDF)
>
> Video S1 (AVI)

AUTHOR INFORMATION

Corresponding Authors

*E-mail: zhangy@iphy.ac.cn.
*E-mail: linzhou@ameslab.gov.

ORCID

Ying Zhang: 0000-0001-5476-1524
Qiang Zheng: 0000-0002-9279-7779
X.-G. Zhang: 0000-0003-0092-5006

Notes

The authors declare no competing financial interest.

ACKNOWLEDGMENTS

We are grateful to S. Z. Lin, Z. Y. Meng, J. Lu, and T. Y. Zhao for their fruitful discussions. This work was supported in part by the U.S. Department of Energy, Office of Science, Basic Energy Sciences, Materials Sciences and Engineering Division, Laboratory Directed Research and Development funds through Ames Laboratory, National Natural Science Foundation of China (11874408, 51590880, 51431009, and 51625101), and Youth Innovation Promotion Association, CAS, 2015004. The authors would like to thank Matt Lynn for TEM sample preparation. All TEM-related work was performed using instruments in the Sensitive Instrument Facility in Ames Laboratory. Ames Laboratory is operated for the U.S. Department of Energy by Iowa State University under contract no. DE-AC02-07CH11358.

REFERENCES

(1) Nagaosa, N.; Tokura, Y. Topological properties and dynamics of magnetic skyrmions. *Nat. Nanotechnol.* **2013**, *8* (12), 899−911.

(2) Neubauer, A.; Pfleiderer, C.; Binz, B.; Rosch, A.; Ritz, R.; Niklowitz, P. G.; Boni, P. Topological Hall effect in the A phase of MnSi. *Phys. Rev. Lett.* **2009**, *102* (18), 186602.

(3) Morikawa, D.; Yu, X.; Karube, K.; Tokunaga, Y.; Taguchi, Y.; Arima, T.-H.; Tokura, Y. Deformation of topologically-protected supercooled skyrmions in a thin plate of chiral magnet $Co_8Zn_8Mn_4$. *Nano Lett.* **2017**, *17* (3), 1637−1641.

(4) Skyrme, T. H. R. A Unified field theory of mesons and baryons. *Nucl. Phys.* **1962**, *31*, 556−569.

(5) Bogdanov, A. N.; Yablonskii, D. A. Thermodynamically stable 'vortices' in magnetically ordered crystals. The mixed state of magnets. *Sov. Phys. JETP.* **1989**, *95*, 101−103.

(6) Mühlbauer, S.; Binz, B.; Jonietz, F.; Pfleiderer, C.; Rosch, A.; Neubauer, A.; Georgii, R.; Böni, P. Skyrmion lattice in a chiral magnet. *Science* **2009**, *323* (6048), 915−919.

(7) Tonomura, A.; Yu, X.; Yanagisawa, K.; Matsuda, T.; Onose, Y.; Kanazawa, N.; Park, H. S.; Tokura, Y. Real-space observation of skyrmion lattice in helimagnet MnSi thin samples. *Nano Lett.* **2012**, *12*, 1673−1677.

(8) Yu, X. Z.; Onose, Y.; Kanazawa, N.; Park, J. H.; Han, J. H.; Matsui, Y.; Nagaosa, N.; Tokura, Y. Real-space observation of a two-dimensional skyrmion crystal. *Nature* **2010**, *465* (17), 901−904.

(9) Yu, X. Z.; Kanazawa, N.; Onose, Y.; Kimoto, K.; Zhang, W. Z.; Ishiwata, S.; Matsui, Y.; Tokura, Y. Near room-temperature formation of a skyrmion crystal in thin-films of the helimagnet FeGe. *Nat. Mater.* **2011**, *10*, 106−109.

(10) Seki, S.; Yu, X. Z.; Ishiwata, S.; Tokura, Y. Observation of skyrmions in a multiferroic material. *Science* **2012**, *336*, 198−201.

(11) Dzyaloshinsky, I. A thermodynamic theory of "weak" ferromagnetism of antiferromagnetics. *J. Phys. Chem. Solids* **1958**, *4*, 241−255.

(12) Moriya, T. Anisotropic superexchange interaction and weak ferromagnetism. *Phys. Rev.* **1960**, *120* (1), 91−98.

(13) Rößler, U. K.; Leonov, A. A.; Bogdanov, A. N. Chiral skyrmionic matter in non-centrosymmetric magnets. *J. Phys. Conf. Ser.* **2011**, *303*, 012105.

(14) Yu, X. Z.; Kanazawa, N.; Zhang, W. Z.; Nagai, T.; Hara, T.; Kimoto, K.; Matsui, Y.; Onose, Y.; Tokura, Y. Skyrmion flow near room temperature in an ultralow current density. *Nat. Commun.* **2012**, 3, 988.

(15) Karube, K.; White, J. S.; Reynolds, N.; Gavilano, J. L.; Oike, H.; Kikkawa, A.; Kagawa, F.; Tokunaga, Y.; Rønnow, H. M.; Tokura, Y.; Taguchi, Y. Robust metastable skyrmions and their triangular-square lattice structural transition in a high-temperature chiral magnet. *Nat. Mater.* **2016**, *15* (12), 1237−1242.

(16) Peng, L.; Zhang, Y.; Wang, W.; He, M.; Li, L.; Ding, B.; Li, J.; Sun, Y.; Zhang, X.-G.; Cai, J.; Wang, S.; Wu, G.; Shen, B. Real-space observation of nonvolatile zero-field biskyrmion lattice generation in MnNiGa magnet. *Nano Lett.* **2017**, *17*, 7075−7079.

(17) Jonietz, F.; Mühlbauer, S.; Pfleiderer, C.; Neubauer, A.; Münzer, W.; Bauer, A.; Adams, T.; Georgii, R.; Böni, P.; Duine, R. A.; Everschor, K.; Garst, M.; Rosch, A. Spin transfer torques in MnSi an ultralow current density. *Science* **2010**, *330*, 1648−1651.

(18) Fert, A.; Reyren, N.; Cros, V. Magnetic skyrmions: advances in physics and potential applications. *Nat. Rev. Mater.* **2017**, *2*, 17031.

(19) Fert, A.; Cros, V.; Sampaio, J. Skyrmions on the track. *Nat. Nanotechnol.* **2013**, *8* (3), 152−156.

(20) Gallagher, J. C.; Meng, K. Y.; Brangham, J. T.; Wang, H. L.; Esser, B. D.; Mccomb, D. W.; Yang, F. Y. Robust zero-field skyrmion formation in FeGe epitaxial thin films. *Phys. Rev. Lett.* **2017**, *118*, 27201.

(21) Zheng, F.; Li, H.; Wang, S.; Song, D.; Jin, C.; Wei, W.; Kovács, A.; Zang, J.; Tian, M.; Zhang, Y.; Du, H.; Dunin-Borkowski, R. E. Direct imaging of a zero-field target skyrmion and its polarity switch in a chiral magnetic nanodisk. *Phys. Rev. Lett.* **2017**, *119*, 197205.

(22) Milde, P.; Köhler, D.; Seidel, J.; Eng, L. M.; Bauer, A.; Chacon, A.; Kindervater, J.; Mühlbauer, S.; Pfleiderer, C.; Buhrandt, S.; Schütte, C.; Rosch, A. Unwinding of a skyrmion lattice by magnetic monopoles. *Science* **2013**, *340* (5), 1076−1080.

DOI: 10.1021/acs.nanolett.8b03553
Nano Lett. 2018, 18, 7777−7783

(23) Oike, H.; Kikkawa, A.; Kanazawa, N.; Taguchi, Y.; Kawasaki, M.; Tokura, Y.; Kagawa, F. Interplay between topological and thermodynamic stability in a metastable magnetic skyrmion lattice. *Nat. Phys.* **2016**, *12*, 62−66.
(24) Wild, J.; Meier, T. N. G.; Pöllath, S.; Kronseder, M.; Bauer, A.; Chacon, A.; Halder, M.; Schowalter, M.; Rosenauer, A.; Zweck, J.; Müller, J.; Rosch, A.; Pfleiderer, C.; Back, C. H. Entropy-limited topological protection of sskyrmions. *Sci. Adv.* **2017**, *3*, No. e1701704.
(25) Nagao, M.; So, Y.-G.; Yoshida, H.; Isobe, M.; Hara, T.; Ishizuka, K.; Kimoto, K. Direct observation and dynamics of spontaneous skyrmion-like magnetic domains in a ferromagnet. *Nat. Nanotechnol.* **2013**, *8* (5), 325−328.
(26) Yu, X. Z.; Shibata, K.; Koshibae, W.; Tokunaga, Y.; Kaneko, Y.; Nagai, T.; Kimoto, K.; Taguchi, Y.; Nagaosa, N.; Tokura, Y. Thermally activated helicity reversals of skyrmions. *Phys. Rev. B: Condens. Matter Mater. Phys.* **2016**, *93* (13), 134417.
(27) Huang, S. X.; Chien, C. L. Extended skyrmion phase in epitaxial FeGe(111) thin films. *Phys. Rev. Lett.* **2012**, *108*, 267201.
(28) Yu, X. Z.; Morikawa, D.; Yokouchi, T.; Shibata, K.; Kanazawa, N.; Kagawa, F.; Arima, T.; Tokura, Y. Aggregation and collapse dynamics of skyrmions in a non-equilibrium state. *Nat. Phys.* **2018**, *14*, 832−836.
(29) Hagemeister, J.; Romming, N.; von Bergmann, K.; Vedmedenko, E. Y.; Wiesendanger, R. Stability of single skyrmionic bits. *Nat. Commun.* **2015**, *6*, 8455.
(30) Richardson, M.; Ingri, N.; Salomaa, P.; Bloom, G.; Hagen, G. The partial equilibrium diagram of the Fe-Ge System in the range 49−72 at. % Ge, and the crystallization of some iron germanides by chemical transport reactions. *Acta Chem. Scand.* **1967**, *21*, 2305−2317.
(31) Ishizuka, K.; Allman, B. Phase measurement of atomic resolution image using transport of intensity equation. *Microscopy (Oxford, U. K.)* **2005**, *54* (3), 191−197.

DOI: 10.1021/acs.nanolett.8b03553
Nano Lett. 2018, 18, 7777−7783